frontiers | Frontiers in Earth Science

TYPE Original Research
PUBLISHED 15 June 2023
DOI 10.3389/feart.2023.1214184

OPEN ACCESS

EDITED BY
Lijie Guo,
Beijing Mining and Metallurgy Technology Group Co., Ltd., China

REVIEWED BY
Lin Chi,
University of Shanghai for Science and Technology, China
Xiaodan Li,
Chongqing Technology and Business University, China

*CORRESPONDENCE
Changlong Wang,
baistuwong@139.com

RECEIVED 29 April 2023
ACCEPTED 05 June 2023
PUBLISHED 15 June 2023

CITATION
Bao P, Jing J, Qi Y, Ma J, Ping H, Wang C, Liu Z, Zheng Y, Zhai Y and Liu F (2023), Firing mechanism and benefit evaluation of high-strength fired water permeable brick containing vanadium-titanium iron ore tailings.
Front. Earth Sci. 11:1214184.
doi: 10.3389/feart.2023.1214184

Firing mechanism and benefit evaluation of high-strength fired water permeable brick containing vanadium-titanium iron ore tailings

Pingju Bao[1], Jianlin Jing[2], Yang Qi[2], Jintao Ma[2], Haoyan Ping[2], Changlong Wang[2]*, Zhibing Liu[2], Yongchao Zheng[3], Yuxin Zhai[4] and Feng Liu[5]

[1]School of Management Engineering and Business, Hebei University of Engineering, Handan, China, [2]Collaborative Innovation Center for Intelligent Regulation and Integrated Management of Water Resources Jointly Built by Provinces and Ministries, School of Civil Engineering, Hebei University of Engineering, Handan, China, [3]Beijing Building Materials Academy of Science Research, State Key Laboratory of Solid Waste Reuse for Building Materials, Beijing, China, [4]China Railway Construction Group Co., Ltd., Beijing, China, [5]Construction Development Co., Ltd., China Railway Construction Group Co., Ltd., Beijing, China

Introduction: The vanadium-titanium iron ore tailings (VTIOTs) has a significant amount of discharge, and serious pollution, which makes it difficult to use directly as a resources resource.

Methods: High-strength fired water permeable brick (HSFWPB) was prepared using VTIOTs as the main raw material. The orthogonal test, X-ray diffraction analysis (XRD), scanning electron microscope (SEM), energy dispersive spectrometry (EDS), and synthetic precipitation leaching procedure (SPLP) were obtained to study the basic properties and firing mechanism of HSFWPB containing VTIOTs, and an economic benefit evaluation was conducted on the project investment of HSFWPB containing VTIOTs.

Results: The results show that when the content of VTIOTs in HSFWPB is 78%, the firing temperature (FT) is 1080°C and the holding time is 120 min, the compressive strength and permeability coefficient of the fired product reach 70.4 MPa and 0.055 $cm \cdot s^{-1}$, respectively, which meet the requirements of Cc60 grade products in *Water permeable brick* (JC/T 945–2005). The products of HSFWPB containing VTIOTs after firing are diopside ($CaMgSi_2O_6$) and augite (Ca (Mg, Fe, Al) (Si, $Al)_2O_6$), with the increase of FT and the extension of HT, the low melting point elements of P, Na, K dissolve out, and the content of Fe and Al in the firing products increases, most of Ca^{2+} in diopside is replaced by Fe^{3+}, so that augite becomes the main crystal phase. With the increase of FT, the pores in the fired products are changed from: closed pores with different sizes→ connected pores with irregular diameters→ irregular collapse pores→ small and uniform circular pores, which provides a guarantee for the permeability of HSFWPB containing VTIOTs.

Discussion: The full investment payback period of the project of HSFWPB containing VTIOTs is 1.77 years. When the production reaches 48.585% of the design output, it reaches a breakeven point, and the project has strong risk resistance ability. The research has improved the utilization rate of VTIOTs and provided a new approach for the large-scale application of VTIOTs.

KEYWORDS

vanadium-titanium iron ore tailings (VTIOTs), high-strength fired water permeable brick (HSFWPB), basic property, firing mechanism, benefit evaluation, augite

1 Introduction

With the increasing exploitation of mineral resources, tailings production has also increased (Jiang et al., 2019; Sun H. Y. et al., 2021). At present, building tailings ponds to store tailings is a common tailings treatment method (Rey et al., 2020; Chen D. Q. et al., 2021). However, tailings ponds occupy a large amount of arable land and forest land, which can easily lead to geological disasters such as landslides and mudslides (Zhao et al., 2020; Li et al., 2021; Li et al., 2022; Peng et al., 2020; Tang et al., 2021). In addition, the harmful substances formed by heavy metal ions in tailings can also pollute the water and soil resources near the tailings pond, affecting normal production and the lives of surrounding residents (Jiang et al., 2018; Wang et al., 2018; Luo L. Q. et al., 2019; Tang et al., 2019). Tailings storage isan optimal solution. Vanadium-titanium iron ore tailings (VTIOTs) are industrial solid waste produced by vanadium-titanium magnetite ore after beneficiation containing element such as Fe, Ti, and V that yet to be recovered, scattered and rare elements such as Co, Ga, and Sc, and possessing high comprehensive utilization value. Presently, the storage of tailings ponds has not realized its potential value, which is also a waste of secondary resources (Li et al., 2020; Zhu et al., 2021; Gan et al., 2022; Huang et al., 2023). Therefore, it is of great significance to promote the comprehensive utilization of VTIOTs for improving resource efficiency, improving environmental quality and promoting the comprehensive transformation of economy and society (Chen et al., 2015; Yu et al., 2019; Zhang et al., 2019; Chen et al., 2021; Sun et al., 2021; Li et al., 2022). In recent years, VTIOTs have been applied to extract valuable metals (Zhang et al., 2019) and prepare building materials, such as foamed ceramics (Xi et al., 2018; Li et al., 2020; Zhu et al., 2021; Li L. et al., 2022), composite cementitious materials (Liu and Zhao, 2020; Wang et al., 2023a), sound insulation panels (Wang C. L. et al., 2022), concrete (Wang and Qin, 2019; Wang C. L. et al., 2021), cement clinker (Yang and Sun, 2020), autoclaved aerated concrete (Shi and Song, 2020), and so on.

Due to the widespread use of cement and asphalt in urban areas, pavement hardening has reduced the exchange of heat and water vapor between the air and ground, leading to an increasing number of environmental problems in cities. The advanced thought and design applied to sponge city construction can conducive to promoting the transformation and development of urban stormwater management mode and guaranteeing the security of water ecosystem (Xu et al., 2018; Nguyen et al., 2019; Guan et al., 2021). Permeable materials are a crucial factor of sponge city construction that can help alleviate the problem of urban rainwater drainage and utilization at the source (Yu et al., 2021; Song, 2022; Qi et al., 2023). Water permeable bricks (WPB), as a type of permeable material with high porosity, breathability, and moisture retention that other road paving materials lack (Wang C. L. et al., 2019; Li J. H. et al., 2021; Wang H. F. et al., 2022; Lv et al., 2022). WPB can infiltrate rainwater into the ground, and there is no obvious runoff in case of rainstorm, achieving the effect of drying when the rain stops. This has played a positive role in the replenishment of soil water and groundwater resources, effectively alleviating the negative impact of hardened roads on urban groundwater resources. The compressive strength (CS) and permeability coefficient (PC) of WPB are generally 30–55 MPa and 1.5×10^{-2}~4×10^{-2} cm·s^{-1}, respectively (Liu et al., 2019; Liu et al., 2020; Cai et al., 2021; Yang et al., 2021). WPB not only meets the mechanical performance requirements of general road surfaces, but its own water permeability, breathability, and water retention also bring many benefits to the urban environment: it can alleviate the heat island effect and urban waterlogging (Asaeda and Ca, 2000; He et al., 2019; Luo et al., 2022; Seifeddine et al., 2022), replenish groundwater (Sansalone et al., 2008; Han et al., 2023), absorb sound and reduce noise (Fang et al., 2022), and achieve comprehensive utilization of waste (Wang Y. G. et al., 2019; Yan et al., 2020). Industrial solid waste contains many inorganic components such as Al_2O_3 and SiO_2 which are high-quality raw materials for preparing WPB products. High-strength fired water permeable brick (HSFWPB) can be prepared by high-temperature firing using solid waste such as coal gangue, waste ceramics, and granulated blast furnace slag (GBFS) as aggregates, clay, shale, or other waste as binders, and appropriate pore forming or foaming agents. Kim et al. (2019) improved the traditional preparation process of WPB, greatly increasing the porosity of WPB, but did not further study the CS, so the practical value of the prepared WPB is relatively low; Xu et al., 2019 selected tailings sand as aggregate and sludge as binder to prepare WPB, but the properties of WPB are not ideal. The main problem is that the binder used in the prepared WPB has poor properties; Luo X. et al., 2019 used tailings and sludge as raw materials, and added shale as an additional binder, but the CS of the fired water permeable bricks (FWPB) samples was low. Wang Z. Y. et al., 2019 prepared WPB with foundation glass as binder and tailing ore as aggregate, but the CS of the WPB did not reach 30 MPa. The above research uses industrial solid waste to prepare WPB, but the performance indicators of the prepared products are low and cannot be applied in industry. In order to further improve the performance of WPB, based on previous research by the research group (Wang S. X. et al., 2021; Ye, 2021), the effects of aggregate content (AC), firing temperature (FT), and holding time (HT) on the basic properties of HSFWPB were studied using VTIOTs as the main raw material and using "three factors and four levels" orthogonal experiments. On this basis, X-ray diffraction (XRD), scanning electron microscope (SEM), and energy dispersive spectrometry (EDS) were used to analyze the effects of HT and FT on the phase composition and mineral transformation of HSFWPB. The firing mechanism of HSFWPB was studied, and the economic benefits of the project investment in HSFWPB containing VTIOTs were evaluated. Prior to this study, various scholars had investigated the effects of process conditions on SWPB. However, there were notable differences in the raw materials used in their studies compared to ours, and the previous trend patterns may not be fully applicable. As a result, our research provides a necessary and comprehensive understanding of the effects of process conditions on SWPB

TABLE 1 Chemical composition of raw materials (wt. %).

Materials	SiO_2	Al_2O_3	Fe_2O_3	CaO	K_2O	MgO	Na_2O	P_2O_5	TiO_2	Other	LOI
VTIOTs	41.13	7.83	11.05	20.38	0.42	12.52	0.54	0.26	0.87	1.90	3.10
LM	51.41	14.32	5.29	5.18	2.12	2.36	0.58	1.84	0.12	2.35	14.43
GTs	62.21	15.14	4.22	3.57	2.83	2.15	3.64	0.12	0.32	1.35	4.45
Shale	56.21	22.15	5.32	2.73	3.20	2.11	1.07	0.43	0.84	1.64	4.30

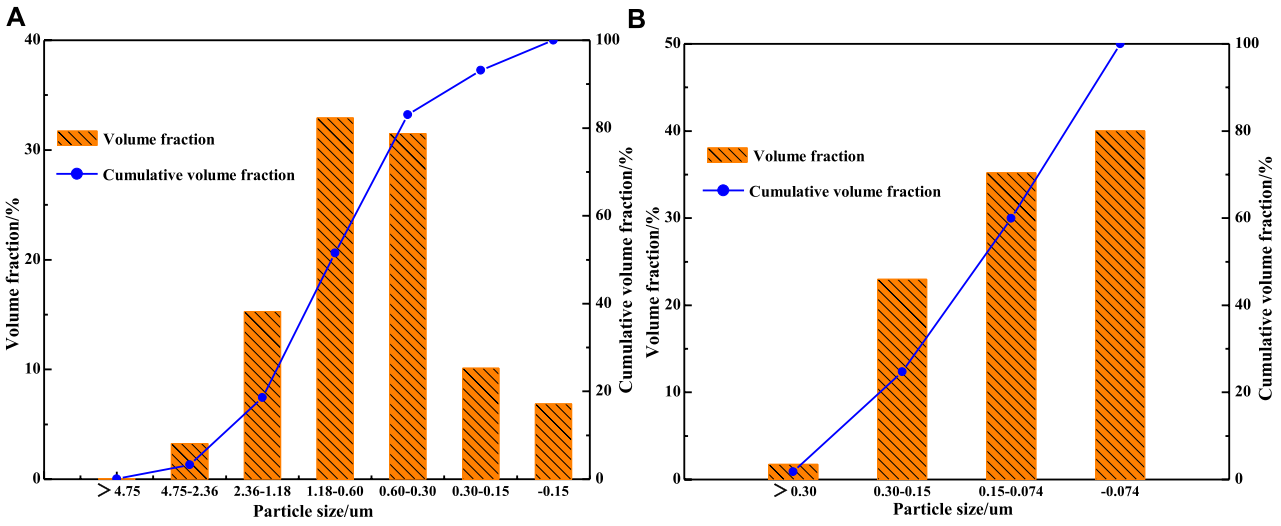

FIGURE 1
Particle size distribution of raw materials. **(A)** VTIOTs, **(B)** GTs.

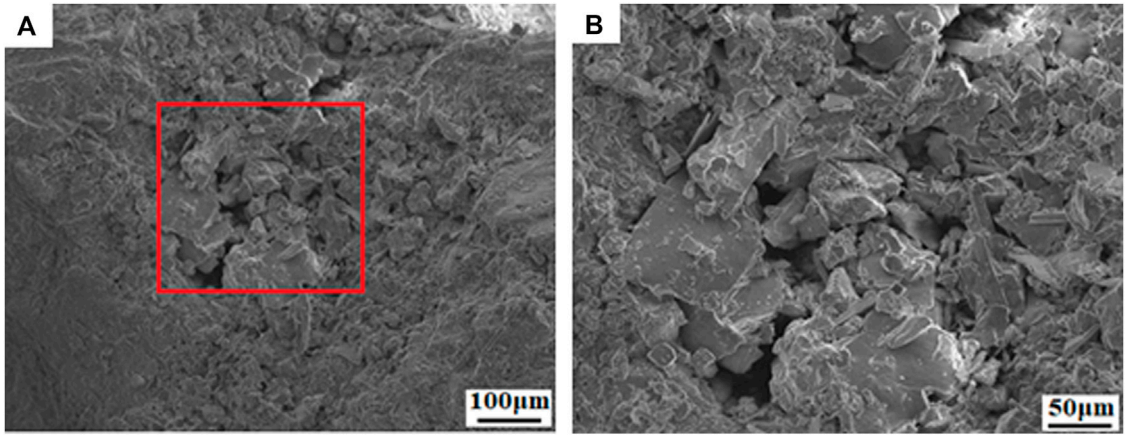

FIGURE 2
SEM images of VTIOTs. **(A)** 500 times; **(B)** 1,000 times.

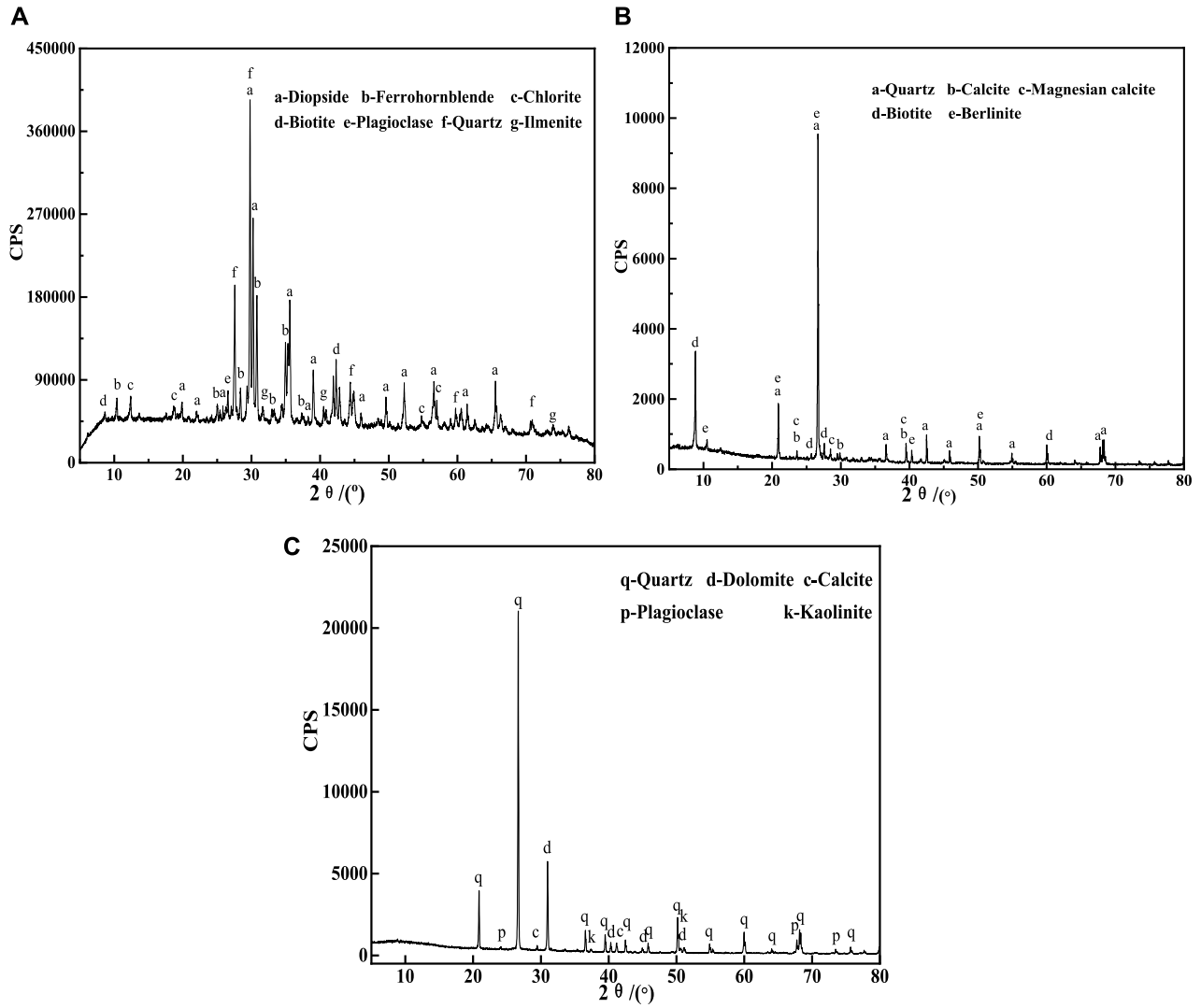

FIGURE 3
XRD patterns of raw materials. **(A)** VTIOTs, **(B)** LM, **(C)** GTs.

using VTIOTs and GTs, which have not been widely studied in the past.

2 Experimental materials and methods

2.1 Experimental materials

The industrial solid waste raw materials used in the preparation of HSFWPB in the study include VTIOTs, lake mud (LM), gold tailings (GTs), and shale. The chemical composition is shown in Table 1.

(1) VTIOTs. The stacking density of VITOs is 1.84 g cm^{-3}, with a particle size range of 0.30–1.18 mm accounting for 64.81%, and particles with a particle size greater than 1.18 mm (see Figure 1A) are beneficial for the formation of pores and expansion of pore size in WPB. From Figure 2, the surface of VITOs particles is rough and the texture is dense. The rough outer surface can provide mechanical interlocking force for the accumulation of particles, and when used as a WPB aggregate, it can form a skeleton structure and form certain pores between the particles, which is conducive to the permeability of the WPB. In addition, the diameters present in the particles range from 50 to 100 μm. The pores can absorb the molten liquid phase generated at high temperatures, which not only promotes the bonding between particles, but also improves the compactness of the structure, providing an important guarantee for the CS of WPB. The main mineral composition of VITOs is silicate minerals, including diopside, biotite, chlorite, quartz, and so on (see Figure 3A). Its chemical composition is mainly CaO, MgO, SiO_2 (see Table 1). Combined with the surface properties of the particles, it can be concluded that VTITOs are conducive to the formation of a MgO-CaO-SiO_2 system and can be used as an ideal firing material.

(2) LM. The LM particles used are fine, with a small number of impurities such as water plants, and the surface is gray with a water content of about 70%. After precipitation and dehydration, the LM is placed in a cool place in the interior for air drying. It is then dried in a drying oven (105°C), and then crushed to −2 mm by rolling. The mixed sample is then placed in a drying oven and dried for 24 h at 105°C. The dried sample obtained is ground to −0.074 mm by an agate grinder for later use. From Table 1, the raw materials of LM are mainly inorganic components, with Al_2O_3 content of 14.32%, SiO_2 content of 51.41%, and organic matter content of approximately 14.43%, indicating that the pyrolysis LM has good gas-production performance. The constituent minerals of LM are: berlinite, biotite, magnesium calcite, calcite, and quartz (see Figure 3B).

(3) GTs. The appearance of GTs was gray, mainly powdery particles with particle size less than 0.30 mm, and the yield below 0.15 mm was 75.24% (see Figure 1B). The main chemical component of GTs is SiO_2, its content is as high as 62.21%, belonging to a high-silicon mineral material. The main mineral composition of GTs is quartz, dolomite, calcite, a small amount of kaolinite and plagioclase (see Figure 3C).

(4) Shale. Shale has a beige appearance and is predominantly powdery with a size of −0.074 mm. The chemical composition of GTs is as follows: SiO_2 accounts for 56.21%, Al_2O_3 accounts for 22.15%, and Fe_2O_3 accounts for 5.32% (see Table 1).

2.2 Experimental method

2.2.1 Preparation of HSFWPB

Firstly, weigh the VITOs aggregate according to the required ratio in the experiment and place it in a cement mortar mixer for 30 s, while adding 5% water; Afterwards, pour the powder with different proportions into the mixer and mix with the aggregate again for 1 min to obtain the mixture used in the experiment; Finally, place the mixture in a sealed bag and age for 12 h. Then, each weighing 500 g aged mixture and place it in the φ75×50 mm mold, press and shape at a corresponding pressure of 25 MPa; Dry the pressed body in a 105°C air dryer for 12 h; Place the dried body into a muffle furnace and burn it into shape under the relevant firing system required by the experiment. The firing system of the pressed body is as follows: First, rising temperature from the room temperature to 60°C, which the heating rate is 0.5°C min^{-1}. Then, the rising temperature from 60°C to 300°C with the heating rate for 2°C min^{-1}. Then increasing the temperature from 300 to 800°C at a rate of 3°C min^{-1}, insulation for 60 min; Finally, rising temperature from 800°C to the required temperature for the experiment (1,050, 1,060, 1,070, 1,080°C), with a heating rate of 1°C min^{-1}, holding for a certain time (60, 90, 120, 150 min), and finally decrease from the highest firing temperature to room temperature with the furnace.

2.2.2 Property characterization

The porosity of HSFWPB was determined by the boiling method in the *Test method for apparent porosity and bulk density of porous ceramic* (GB/T 1966-1996); The flexural strength (FS), splitting tensile strength (STS) and PC of HSFWPB were determined according to the method specified in Appendix A, B and C of *Permeable paving bricks and permeable paving flags* (GB/T 25993-2010); The determination of CS of HSFWPB was carried out according to the method in Appendix A of *Water permeable brick* (JC/T 945-2005). SPLP was conducted to test the leaching behavior of heavy metals in HSFWPB containing VTIOTs, thus confirming the environmental safety. The phase composition of HSFWPB was analyzed using a German Bruker D8 Advance X-ray diffractometer under operating conditions of voltage 40 kV, current 30 mA, Cu target, 2 θ range 10°–90°, step size 0.02°, scanning rate 8° min^{-1}; Through the Zeiss SUPRA™55 scanning electron microscope coupled with a Be4-U92 energy spectrum, SEM observation was performed to analyze the microstructure of HSFWPB samples.

3 Results and discussion

3.1 Basic properties of HSFWPB containing VTIOTs

3.1.1 Orthogonal design of HSFWPB

The research aims to improve the comprehensive utilization rate of VTIOTs and minimize energy consumption, to prepare HSFWPB that meet the requirements of *Permeable paving bricks and permeable paving flags* (GB/T 25993-2010) and *Water permeable bricks* (JC/T 945-2005). Therefore, based on previous research (Wang C. L. et al., 2021; Ye, 2021), the undisturbed VTIOTs were sieved into three particle size ranges: 1.18–4.75 mm (coarse particle size), 0.60–1.18 mm (medium particle size), and 0.15–0.60 mm (fine particle size). The measured stacking densities were 1.56 g·cm^{-3}, 1.58 g·cm^{-3}, and 1.76 g·cm^{-3}, respectively. Due to the main particle size range of VTIOTs from 0.60 to 1.18 mm ensure high utilization of VTIOTs, the medium particle size was selected as the main particle size, and other particle sizes were studied. The ratio of GTs, LM and shale in the binder was 2: 2: 1. Optimize the mix proportion and property of HSFWPB using orthogonal experiments. Three main factors of AC (represented by A), FT (represented by B) and HT (represented by C), were selected in orthogonal experiments, with four level values taken for each factor. The levels of AC are selected 77%, 78%, 79%, and 80%, and FT are 1,050, 1,060, 1,070, and 1,080°C, HT are 60, 90, 120, and 150 min.

3.1.2 Results and analysis of orthogonal experiment for HSFWPB

The test results of PC, and CS for HSFWPB containing VTIOTs in the orthogonal experiment are shown in Table 2. WPB fired from VTIOTs has the potential for high strength and high permeability. When the AC is between 77% and 80%, the PC variation range of HSFWPB are 0.058–0.118 cm s^{-1}, the CS is reduced from 67.5 MPa to 36.3 MPa, and its PC and CS meet the requirements of Cc35 grade products in the *Water permeable brick* (JC/T 945-2005). At the same time, its PC meets the requirement of Grade A product in *Permeable paying bricks and permeable paying flags* (GB/T 25993-2010), its PC value is greater than or equal to 0.02 cm·s^{-1}. PC and CS are two opposing performance indicators. When the AC increases, the internal porosity of HSFWPB increases, which enhances the water permeability. The overall density of HSFWPB decreases, leading to a decrease in CS. Therefore, the most excellent combination of CS for HSFWPB containing VTIOTs is $A_1B_4C_4$, the combination that only considers the best PC is $A_4B_1C_4$.

The range analysis method for orthogonal experimental is to solve the existing problems by using the average range of each pair of

TABLE 2 Orthogonal test scheme and results for HSFWPB containing VTIOTs.

Number	Factor			Test scheme	PC/(cm·s^{-1})	CS/MPa
	A (AC/%)	B (FT/°C)	C (HT/min)			
1	1(77%)	1(1,050°C)	1(60 min)	$A_1B_1C_1$	0.108	40.2
2	1(77%)	2(1,060°C)	2(90 min)	$A_1B_2C_2$	0.093	49.6
3	1(77%)	3(1,070°C)	3(120 min)	$A_1B_3C_3$	0.080	60.7
4	1(77%)	4(1,080°C)	4(150 min)	$A_1B_4C_4$	0.058	67.5
5	2(78%)	1(1,050°C)	2(90 min)	$A_2B_1C_2$	0.114	38.1
6	2(78%)	2(1,060°C)	1(60 min)	$A_2B_2C_1$	0.099	42.2
7	2(78%)	3(1,070°C)	4(150 min)	$A_2B_3C_4$	0.076	58.3
8	2(78%)	4(1,080°C)	3(120 min)	$A_2B_4C_3$	0.061	65.7
9	3(79%)	1(1,050°C)	3(120 min)	$A_3B_1C_3$	0.116	37.6
10	3(79%)	2(1,060°C)	4(150 min)	$A_3B_2C_4$	0.087	44.2
11	3(79%)	3(1,070°C)	1(60 min)	$A_3B_3C_1$	0.089	45.4
12	3(79%)	4(1,080°C)	2(90 min)	$A_3B_4C_2$	0.078	58.5
13	4(80%)	1(1,050°C)	4(150 min)	$A_4B_1C_4$	0.118	36.3
14	4(80%)	2(1,060°C)	3(120 min)	$A_4B_2C_3$	0.113	38.7
15	4(80%)	3(1,070°C)	2(90 min)	$A_4B_3C_2$	0.086	42.5
16	4(80%)	4(1,080°C)	1(60 min)	$A_4B_4C_1$	0.083	44.6

TABLE 3 Range analysis of PC and CS for HSFWPB containing VTIOTs.

Property index	Factor	A (AC/%)	B (FT/°C)	C (HT/min)
PC/(cm·s^{-1})	$\bar{k}_1$	0.08475	0.114	0.09475
	$\bar{k}_2$	0.0875	0.098	0.09275
	$\bar{k}_3$	0.0925	0.08275	0.0925
	$\bar{k}_4$	0.1	0.07	0.08475
	R_1	0.01525	0.044	0.01
CS/MPa	$\bar{k}_1$	54	37.75	42.75
	$\bar{k}_2$	50.75	43.25	46.75
	$\bar{k}_3$	46	51.25	50
	$\bar{k}_4$	40	58.5	51.25
	R_2	14	20.75	8.5

influencing factors. An increase in the range indicates that this element has a more significant impact on the experimental results, while a decrease in the range indicates that the impact is not significant. Table 3 shows the range analysis results of the orthogonal test. R_1 and R_2 represent the average range of PC and CS for HSFWPB containing VTIOTs, respectively in Table 3. The main and secondary factors affecting the PC of HSFWPB are as follows: FT > AC> HT. The PC of HSFWPB containing VTIOTs increases with the increase of AC content, and gradually decreases as FT and HT increase; The CS decreases with the increase of AC content, and further increases with the increase of FT and HT. Therefore, the $A_4B_1C_1$ is considered as the optimal experimental plan for HSFWPB containing VTIOTs that only consider PC. The $A_1B_4C_4$ is considered the optimal experimental for HSFWPB, that only considers CS. Due to the conflict between the two property indicators, further analysis of variance is required to achieve the optimal experimental plan with ideal balance (see Table 4).

It can be seen from the variance analysis of HSFWPB's PC in Table 4 that the test statistics of AC, FT and HT are 0.26, 0.21, and 0.12, respectively. Therefore, the main and secondary affecting factors on the PC of HSFWPB are as follows: AC > FT > HT. Since the test statistics of all factors are less than the critical value, the influence of factors on the PC is not significant. The influence level factors among the insignificant factors can be selected from the perspective of cost reduction. According to the variance analysis of HSFWPB's CS, the test statistics of AC, FT and HT are 35.05, 78.21, and 13.65, respectively. Therefore, the main and secondary factors affecting the CS of HSFWPB are as follows: FT> AC> HT. Since the test statistics of each factor are greater than the critical value, each factor has a significant impact on CS. The level of significant factors should be the best level. In summary, the best combination of various factors is $A_1B_4C_4$, which means that the AC is 77%, the HT is 1,080°C, and the HT is 150 min. The prepared HSFWPB containing VTIOTs has a PC and CS of 0.058 cm·s^{-1} and 67.5 MPa, respectively. However, the combination scheme of $A_2B_4C_2$ on property indicators in Table 2 are not significantly different from $A_1B_4C_4$, its PC and CS in $A_2B_4C_2$ reach 0.061 cm·s^{-1} and 65.7 MPa, respectively. In the combination scheme of $A_2B_4C_2$, the AC, HT, and HT of HSFWPB containing VTIOTs are 78%, 1,080°C, and 120 min, respectively. From

TABLE 4 Variance analysis table of PC and CS for HSFWPB containing VTIOTs.

Property index	Variance source	Sum of squares of deviations	Freedom	Mean square	Test statistic	Critical value	Significance
PC	AC	0.00054	3	0.000180	0.26	$F_{0.05}(3,6)=4.76$	non significant
	FT	0.00044	3	0.000147	0.21	$F_{0.25}(3,6)=1.78$	non significant
	HT	0.00024	3	0.000080	0.12		non significant
	Error	0.00412	6	0.000687			
	Sum	0.00534	15	—			
CS	AC	444.6875	3	148.229	35.05	$F_{0.05}(3,6)=4.76$	significant
	FT	992.1875	3	330.729	78.21	$F_{0.25}(3,6)=1.78$	significant
	HT	173.1875	3	57.729	13.65		significant
	Error	25.375	6	4.229			
	Sum	1,635.4375	15	—			

TABLE 5 Different mix proportion of binder and property indicators for HSFWPB containing VTIOTs.

Number			A	B	C	D	E	F	G
Binder composition/%	GT		1	1	1	1	2	2	2
	LM		1	2	1	2	1	2	1
	Shale		1	1	2	2	1	1	2
Properties indicators	Porosity/%		23.29	24.94	23.15	23.21	22.61	24.55	22.45
	PC/(cm·s^{-1})		0.069	0.078	0.063	0.058	0.055	0.061	0.066
	CS/MPa		68.2	60.6	69.4	66.5	70.4	65.7	69.0
	FS/MPa		12.9	11.7	13.2	12.6	13.5	12.5	13.0
	STS/MPa		4.9	4.5	5.2	4.6	5.4	4.7	5.1
	WQ/mm		31	35	29	32	26	33	30
	FR	CSFC/MPa	62.7	55.2	64.0	61.1	65.1	60.3	63.5
		CSLR/%	8.06	8.91	7.78	8.12	7.53	8.22	7.97

Note: WR (Water retention); WQ (wear quality); FR (freezing resistance); CSFC (compressive strength after 25 freeze-thaw cycles); CSLR (loss rate of compressive strength after 25 freeze-thaw cycles).

the perspective of comprehensive utilization rate and energy consumption reduction of VTIOTs, the PC and CS of the $A_2B_4C_2$ meet the requirements of Cc60 grade products in *Water permeable brick* (JC/T 945-2005), and its PC meets the requirements of A-grade products in GB/T 25993-2010.

3.2 Properties of HSFWPB containing VTIOTs under optimal conditions

3.2.1 Effect of binder mix ratio on the properties of HSFWPB containing VTIOTs

Binders are important materials used to bond aggregates and form a certain mechanical strength. It binds particles to each other, enhance the bonding degree of WPB and plays a crucial role in improving the strength of WPB, ensuring product yield, and reducing FT. The appropriate mix proportion of the binder can transfer and fully encapsulate the aggregate in a molten state, and provide important guarantees for various properties. The orthogonal experimental study on aggregate content in Section 3.1.2 shows that the various property indicators of HSFWPB containing VTIOTs are relatively ideal in the content of 78%. Therefore, this section selects an aggregate content of 78%, a binder content of 22%, a FT of 1,080°C, and a HT of 120 min to explore the influence of the binder mix proportion on the physical property indicators of WPB. The binders with different mix proportions and corresponding property indicators are shown in Table 5.

Table 5 shows the property indicators of HSFWPB with different binder mix proportions. From the PC and porosity, it can be seen

that the two property indicators correspond to each other and present a certain regularity, that is, when the porosity decreases, the PC also decreases accordingly, is that, the porosity decreases with the decrease of PC. According to the research in Section 3.1, it can be preliminarily understood that when the permeability of the adobe increases, its related mechanical property indicators decrease, such as CS, FS, and STS. Compared to this, the permeability and mechanical properties didn't show corresponding regularity in different binder mix proportions. The reason for this is that there is a significant difference in the properties of different binders in high-temperature melting conditions. The number of pores is directly determined by the amount of liquid phase formed. The more liquid phase there is, the less pores there are, leading to a decrease in PC and porosity. However, the amount of liquid phase formed does not necessarily indicate that the binder has sufficient adhesion, so it presents different macroscopic intensities. Among all groups, E group showed the best property, with a porosity of 22.61%, a PC of 0.055 $cm \cdot s^{-1}$, CS, FS, and STS are respectively 70.4, 13.5, and 5.4 MPa and with a wear quality (WQ) of 26 mm. The maximum strength loss rate after 25 freeze-thaw experiments is 7.53% which is far less than the 20% required in the *Water permeable brick* (JC/T 945–2005) and *Permeable paving bricks and permeable paving flags* (GB/T 25993-2010). C, D, and G groups can be seen that when the shale content is high, the porosity is higher compared to other groups, and the liquid phase generated at FT of 1,080°C is less, which is not conducive to the mechanical properties of HSFWPB containing VTIOTs. Therefore, from this perspective, the shale content should not be too high. In addition, from B, D, and F groups, it can be seen that the property indicators of HSFWPB containing VTIOTs are relatively low, because the FT of LM is relatively high, and it cannot achieve the best bonding property at 1,080°C.

3.2.2 Environmental impact of HSFWPB containing VTIOTs

At present, one of the focuses of industrial solid waste application research is its application in the field of building materials, but little attention is attached to its heavy metal leaching problem. VTIOTs, GTs, LM and shale, as the industrial solid waste and the corresponding building materials, contain Cr, Zn, Cu, Ni, Pb, Cd, As and other heavy metals (Zhang et al., 2018; Young et al., 2021; Sarathchandra et al., 2022). They are easy to transfer and transform in the environment, presenting potential environmental risks. During SPLP, the leach liquor was prepared by adding 60%/40% (mass fraction) of sulfuric acid/nitric acid and diluting appropriately with deionized water, in order to adjust the pH to 4.20 ± 0.05 (Wang et al., 2023b; Zhang et al., 2023). The leach liquor and solidified powder (<0.075 mm) were mixed according to the ratio of 20:1, and shaken for 18 h in a gyrate shaker. Then, the screened mixture (0.45 μm) was put into Prodigy 7 Inductively coupled plasma emission spectrometer (ICP-OES) to analyze the concentration of Cr, Ni, Cu, Cd, Pb, Zn, As, and Hg (Wang et al., 2023c).

In this study, the leaching toxicity of HSFWPB raw materials (VTIOTs, GTs, LM, and shale), and HSFWPB samples were separately tested by the SPLP test. HSFWPB was prepared from 78% VTIOTs and 22% binder (GTs: LM: shale=2: 1: 1) at a FT of 1,080°C and a HT of 120 min. A block of HSFWPB sample was prepared into a powder after drying. The test results are shown in Table 6.

From Table 6, it can be seen that compared to the relevant national standards of heavy metal leaching concentration, the heavy metal leaching concentration in HSFWPB products and the raw materials used for their preparation can meet the standard values of Class II water quality required in the *Technical specification for collaborative disposal of solid waste in cement kilns* (GB 30760-2014) and *Environmental quality standards for surface water* (GB3838-2002). At the same time, it also meets the standard value requirements for Class III water quality in the *Standard for groundwater quality* (GB/T14848-2017) and the standard value requirements in the *Identification standards for hazardous wastes- Identification for extraction toxicity* (GB 5085.3-2007). Therefore, HSFWPB containing VTIOTs can be used as building materials, and their heavy metal leaching concentration meets environmental safety requirements.

3.3 Composition and structure of HSFWPB containing VTIOTs

3.3.1 Phase composition of HSFWPB containing VTIOTs

Figure 4 shows the phase composition of HSFWPB containing VTIOTs under different conditions. Figure 4A shows the XRD patterns of HSFWPB containing VTIOTs at the FT of 1,080°C and the HT of 60, 90, 120, and 150 min. Figure 4B shows the XRD pattern of HSFWPB when the HT is 120 min and the FT is 1,050, 1,060, 1,070, and 1,080°C. A block of HSFWPB sample is prepared into a powder after drying and its mineral composition is tested by XRD.

As can be seen from Figure 4A, the main mineral phases in HSFWPB containing VTIOTs are diopside and augite ($Ca(Mg Fe,Al)(Si,Al)O_6$). The "steamed bun peak" isobserved in the 2θ range of 25°–35°, indicating the presence of a certain amount of glass phase in the HSFWPB, which increases with the extension of HT. The diffraction peaks at 2θ values of 27.54°, 29.86°, 30.36°, and 35.72° are augite. With the extension of HT, augite increases, while diopside decreases gradually. The reason for this trend is that with the extension of HT, more molten liquid phase is produced in the system, and the molten Fe^{3+} and Al^{3+} produced in the system gradually displace Ca^{2+} in diopside to form augite. The liquid phase in the system bonded with the remaining solid particles and crystals, making the structure dense. Therefore, the CS of the HSFWPB containing VTIOTs continuously increases with the extension of HT, while the PC gradually decreases.

Figure 4B shows that the HSFWPB system is mainly composed of MgO-CaO-SiO_2 ternary system. As the FT rises, the MgO, CaO and SiO_2 in the system react to produce diopside, which in turn combines with Fe^{3+} and Al^{3+} in the liquid phase of the system to transform into augite. The reaction is shown in Eqs 1, 2.

$$MgO + CaO + 2SiO_2 \xrightarrow{1000 \sim 1130℃} Ca_2MgSiO_6\,(\text{diopside}) \quad (1)$$

$$Ca_2MgSiO_6 + Fe^{3+} + Al^{3+} \xrightarrow{1000 \sim 1130℃} Ca\,(Mg, Fe, Al)\,(Si, Al)_2O_6\,(\text{augite}) \quad (2)$$

TABLE 6 The leaching concentrations of heavy metals from some raw materials and HSFWPB containing VTIOTs (μg/L).

Materials	Cu	Pb	Zn	Ni	Cd	Cr	As	Hg
VTIOTs	19.33	0.85	63.31	0.8830	0.4231	0.879	2.5215	0.00224
GTs	20.23	0.92	72.14	1.1384	0.4818	0.964	2.9382	—
LM	5.637	1.36	30.39	0.4538	0.5421	0.948	1.8525	0.04356
Shale	26.161	0.16	37.71	0.0110	0.0908	1.176	0.6716	0.00224
HSFWPB	28.353	1.52	46.93	0.6915	0.4518	0.783	2.3845	0.03618
Limiting value	100	5	100	5	1	5	5	0.1

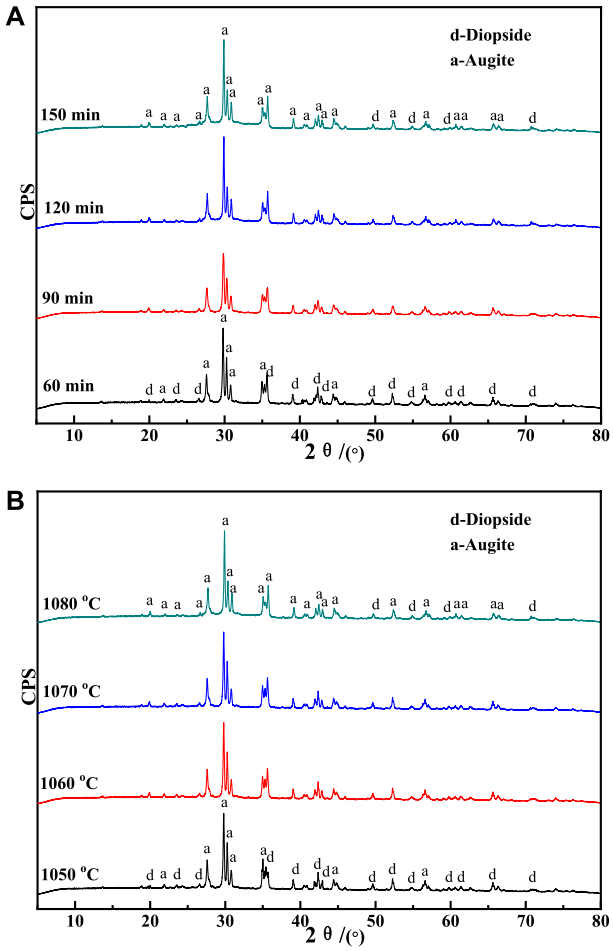

FIGURE 4
XRD patterns of HSFWPB containing VTIOTs. **(A)** Different HT; **(B)** Different FT.

When the FT reaches 1,060°C, a certain amount of molten glass phase is generated in the system, which promotes the migration of crystals under the action of capillary force, and the particles are arranged towards a higher packing density. Currently, the HSFWPB has better mechanical properties on a macro level. When the FT is 1,070°C, the diopside in the system is further combined and transformed with liquid phase ions, which makes the solid particles in the system precipitate again, thus making the material migrate again, and the density of the structure constantly strengthened.

When the FT is 1,080°C, the continuous pores inside the HSFWPB begin to turn into isolated pores. If the FT is further increased, the permeability of the HSFWPB will decrease rapidly. When the FT reaches 1,060–1,080°C, the mineral phase composition inside the HSFWPB with VTIOTs is augite, which indicates that a large amount of liquid phase has been produced in the system at this time, and the porosity has sharply decreased. Although the structure is dense, the production of a large amount of liquid phase makes the particle skeleton peristaltic. The internal structure of the HSFWPB begins to deform and the strength and porosity decrease gradually.

3.3.2 Microstructure of HSFWPB containing VTIOTs

3.3.2.1 SEM analysis

Figure 5 shows SEM images of HSFWPB containing VTIOTs at different levels of HT and FT. HSFWPB samples are prepared from 78% VTIOTs and 22% binder (GTs: LM: shale=2: 1: 1). The HT is 120 min and the FT is 1,050, 1,060, 1,070, and 1,080°C, the porosity of four HSFWPB samples obtained are 24.82%, 24.14%, 23.63%, and 22.61%, respectively. When the FT is 1,050°C, a large number of unconnected and irregularly shaped pores (yellow area in Figure 5A) are generated in the HSFWPB. The surface of the fired product is layered with a tendency to form short columns, indicating that at this time, the crystal of the HSFWPB begins to transform and diopside and a small amount of augite are gradually formed. In Figure 5B, where the HSFWPB is FT 1060°C and the HT is 120 min, the fired products of the HSFWPB gradually become denser, and the short columnar crystals on the surface gradually grow into elongated rod-like clusters. With the changes in the morphology of the fired products, the connected holes with irregular pore sizes are formed in the firing system, which improves the permeability of the HSFWPB.

When the FT reaches 1,070°C (Figure 5C), the round "water droplet" like glass phase appears as a chain bond, forming a skeleton. Meanwhile, irregular collapse holes appear in the visual field, which should be the collapse formed after liquid phase condensation formed by high-temperature melting. In Figure 5D (FT 1080°C, HT 120 min), the internal structure of the HSFWPB begins to deform, leading the formation of many micrometer-level round "water drop" glass-like grains, with some grains agglomerate together to form aggregates. The pore size of the system also reduces, becoming more homogeneous, with a pore size of about 3–5 μm. The whole system is denser, which guarantees the CS and water permeability of HSFWPB. As observed from the comparison shown in Figure 5, the change in FT results in a

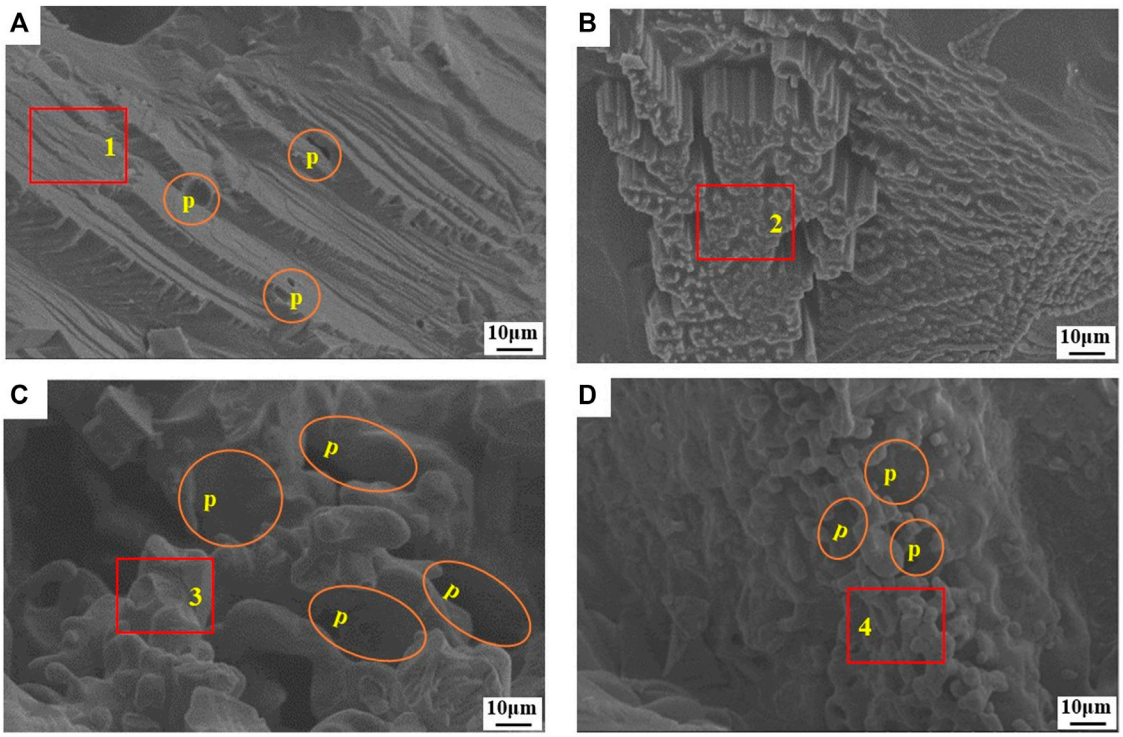

FIGURE 5
SEM images of HSFWPB containing VTIOTs at different FT. **(A)** 1,050°C; **(B)** 1,060°C; **(C)** 1,060°C; **(D)** 1,080°C.

transition of the pores in the fired products, from closed pores of different sizes to connected pores with irregular diameters, to irregular collapse pores, and lastly, to small uniform circular pores, meanwhile, the porosity in fired products also changes from high to low with the increase of FT. This change in trend provides a guarantee for the permeability of HSFWPB.

3.3.2.2 EDS analysis

Figure 6 shows the EDS spectrums of HSFWPB containing VTIOTs. Figure 6A~ Figure 6D correspond to marked region 1–4 in Figure 5.

As shown in Figure 6A, when the HT is 120 min and the FT is 1,050°C, HSFWPB containing VTIOTs products are mainly composed of Ca, Si, Mg and a small amount of Fe and Al elements. The proportion of its main elements is close to that of $CaMgSi_2O_6$. Combined with Figure 4, it is analyzed that the mineral is diopside. Diopside is a one-dimensional chain structure, and its single-chain structure is an infinitely long chain with $[Si_2O_6]^{4-}$ as the structural unit. Compared with Figure 6A, the marked region in Figure 6B showed no change in the types of elements, but the contents of Fe and Al increased, and the proportion of major elements was close to $Ca(Mg, Fe, Al)(Si, Al)_2O_6$. Combined with Figure 4, the mineral was analyzed as augite. The elongated rod-like objects seen in the SEM image of Figure 5B are clusters of augite.

In Figure 6C, low-melting point elements such as P, Na, and K, indicating the presence of a certain amount of liquid phase. A large number of molten glass phases gradually grow in the liquid phase and transform into augite, combined with a part of Fe and Al elements. This finding is consistent with the SEM analysis shown in Figure 5C. In Figure 6D, where the FT is 1,080°C, the content of Fe and Al elements increases, resulting in an increase in the formation of augite. Fe element increases significantly, while the Ca element decreased, indicating that most Ca^{2+} in diopside is replaced by Fe^{3+} at this stage, and diopside changes to augite, making augite the main crystalline phase. Ti element in Figure 6D is the "nucleating agent" of high-temperature fired products (Wang Z. Y. et al., 2019; Zhang et al., 2021; Liu et al., 2023). The presence of Ti element can effectively promote the nucleation of the fired product system, which is conducive to the preparation of high-strength fired products, which also verifies the formation of micron-sized grains in Figure 5D.

3.4 Economic benefit evaluation on HSFWPB containing VTIOTs

3.4.1 Cost analysis

It is planned to build a factory covering an area of 40,000 m^2 with an annual production scale of 400,000 tons of HSFWPB. The optimal ratio $A_2B_4C_2$ of HSFWPB was selected to calculate the raw material cost and freight cost, energy consumption cost, management and wage and welfare cost, plant and facility construction cost (see Table 7).

3.4.2 Economic benefit analysis

Economic benefit analysis includes sales revenue and revenue estimates. According to the sale price of HSFWPB on the market, 30–50 CNY·m^{-2}, equivalent to 240 CNY·t^{-1}, the lowest price of HSFWPB is 240 CNY· t^{-1}, and the annual sales income will be

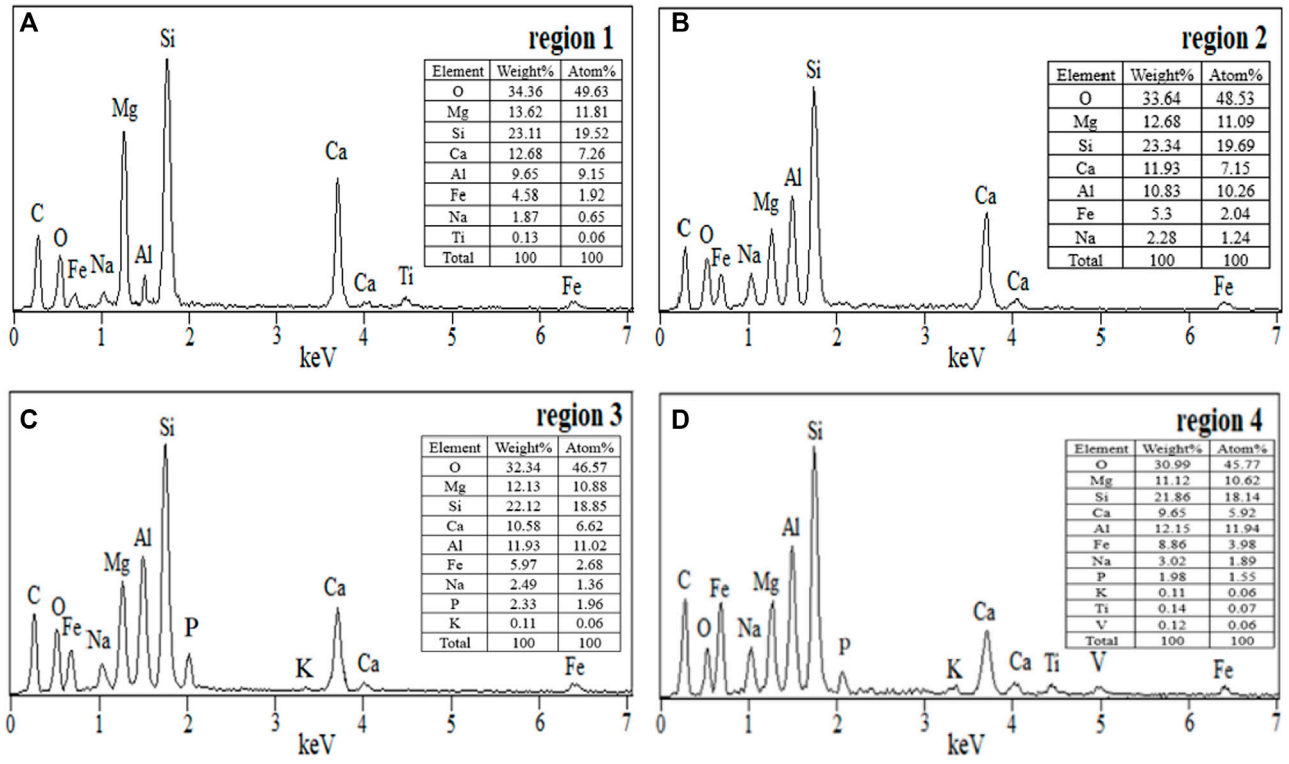

FIGURE 6
EDS spectrums of marked region 1–4 in the Figure 5. **(A)** region 1; **(B)** region 2; **(C)** region 3; **(D)** region 4.

TABLE 7 Cost estimation for the production project of HSFWPB containing VTIOTs (10,000 CNY).

Number	Item		Cost estimation
1	Raw material cost and freight cost	raw material cost	756.2
2		freight cost	2000
3	Energy consumption cost	electricity consumption	488
4		natural gas	1,440
5	Management, salary and welfare costs	employee salaries and welfares	100
6		Production workshop management fee	84
7	Construction cost of factory building and facility	construction cost of the factory building	800
8		equipment cost	1,200
9		depreciation expenses for factory buildings	26.7
10		depreciation expenses for equipment	120
Total			7,014.9

9,600 CNY. According to the relevant policies of our country, enterprises comprehensively use solid waste can be exempt from paying environmental protection tax. When the utilization rate of solid waste reaches more than 30%, value-added tax and the income tax of previous 5 years can be reduced, and the proceeds of the projects are shown in Table 8.

Return on investment=(annual average total profit/total project investment)×100%=(4585.1÷7014.9) × 100%=65.3%.

Profits and taxes on investments=(annual total profit and tax/total project investment)×100%=(5492.9÷7014.9) × 100%=78.3%.

In conclusion, the investment in the production project of HSFWPB containing VTIOTs shows good economic benefits, with a higher return on investment profit and taxes on investments compared to the average industry profit rate (14%) and average profit and tax rate (22%). The economic parameters are summarized in Table 9 to obtain the project investment cash flow statement.

TABLE 8 Project income statement of HSFWPB containing VTIOTs (10,000 CNY).

Number	Item	Capital construction period	Production period				
			Tax reduction period				Non tax reduction period
	Year	1	2	3	4	5–6	7–11
1	Sale income		9,600	9,600	9,600	9,600	9,600
2	Total cost	2000	5,014.9	5,014.9	5,014.9	5,014.9	5,014.9
3	Profit	0	4,585.1	4,585.1	4,585.1	4,585.1	4,585.1
4	Income tax	0	0	0	0	0	1,513.1
5	after-tax profits	0	4,585.1	4,585.1	4,585.1	4,585.1	3,072

Note: after-tax profits= sale income-total cost-income tax (The income tax rate is calculated at 33% of gross profit).

TABLE 9 Project investment cash flow statement of HSFWPB (10,000 CNY).

Year	1	2	3	4	5	6	7	8	9	10	11
Raw material cost		2,756.2	2,756.2	2,756.2	2,756.2	2,756.2	2,756.2	2,756.2	2,756.2	2,756.2	2,756.2
Energy cost		1928	1928	1928	1928	1928	1928	1928	1928	1928	1928
Salary		100	100	100	100	100	100	100	100	100	100
Depreciation expense		146.7	146.7	146.7	146.7	146.7	146.7	146.7	146.7	146.7	146.7
Management expenses		84	84	84	84	84	84	84	84	84	84
Fixed assets	2000										
Sale income		9,600	9,600	9,600	9,600	9,600	9,600	9,600	9,600	9,600	9,600
Cash outflow	2000	5,014.9	5,014.9	5,014.9	5,014.9	5,014.9	5,014.9	5,014.9	5,014.9	5,014.9	5,014.9
Cash inflow	0	9,600	9,600	9,600	9,600	9,600	9,600	9,600	9,600	9,600	9,600
Profit	0	2,585.1	4,585.1	4,585.1	4,585.1	4,585.1	4,585.1	4,585.1	4,585.1	4,585.1	4,585.1
Income tax	0	0	0	0	0	0	1,513.1	1,513.1	1,513.1	1,513.1	1,513.1
Net profit	0	2,585.1	2,585.1	2,585.1	2,585.1	2,585.1	3,072	3,072	3,072	3,072	3,072
Net Cashflow	−2000	2,585.1	2,585.1	2,585.1	2,585.1	2,585.1	3,072	3,072	3,072	3,072	3,072
Accumulated cashflow	−2000	585.1	3,170.2	5,755.3	8,340.4	10925.5	13997.5	17069.5	20141.5	23213.5	26285.5

The full investment payback period is: 1 + 2,000 ÷ 2,585.1=1.77 (year), All investments in the production project of HSFWPB containing VTIOTs can be quickly recovered in 1.77, indicating that the unit investment has reached the average level of the industry and the investment risk is relatively small.

In normal production years when the project reaches the design capacity and the production load reaches 100%, the total cost is 50.149 million CNY, of which the total annual fixed cost is 29.029 million CNY, the annual variable cost is 21.12 million yuan and the annual sales tax is 15.131 million CNY.

Utilization rate of production capacity = annual fixed cost/(annual sales revenue - annual variable cost - annual sales tax) × 100%=2,902.9÷(9,600−2,112−1,513.1) × 100% = 48.58%

Break-even production = designed production capacity × production capacity utilization rate = 400,000% × 48.58% = 194,320 tons.

The calculation results show that when the production capacity of the project is 194,432 tons, that is, when it reaches 48.585% of the designed output, the project will not lose money, so it has substantial risk resistance ability. The raw materials used in the HSFWPB containing VTIOTs products prepared in this project are all industrial solid wastes. Compared with the FWPB products studied by He et al. (2023) and Kong et al. (2022) the FT of the HSFWPB containing VTIOTs product is only 1,080°C, while the FT of FWPB products from He et al. (2023) and Kong et al. (2022) are 1,180 °C and 1,090°C, respectively, and their property indicators are much lower than those of the products in this project. Therefore, the

energy consumption of HSFWPB containing VTIOTs products is lower than that of FWPB products studied by He et al. (2023) and Kong et al. (2022). So the investment in HSFWPB containing VTIOTs products is feasible.

4 Conclusion

(1) HSFWPB was prepared using VTIOTs as the main raw material. When the content of VTIOTs is 78%, the multi-source solid waste binder accounts for 22% (GTs: LM: shale=2:1:1), forming pressure is 25 MPa, FT is 1,080°C and HT is 120 min, CS and PC of HSFWPB can reach 70.4 MPa and 0.055 $cm \cdot s^{-1}$, respectively, which meet the requirements of Cc60 grade products in *Water permeable brick* (JC/T 945–2005). Meanwhile, the PC reaches the requirements of grade A products in *Permeable paving bricks and permeable paving flags* (GB/T 25993–2010).

(2) The products of HSFWPB containing VTIOTs after firing are diopside ($CaMgSi_2O_6$) and augite ($Ca(Mg,Fe,Al)(Si,Al)_2O_6$). With the increase of FT and the extension of HT, the low melting point elements such as P, Na, K dissolve out, and the content of Fe and Al in the firing products increases. Most of Ca^{2+} in diopside is replaced by Fe^{3+}, so that augite becomes the main crystal phase. With the increase of FT, the changes in the pores of the fired products provide a guarantee for water permeability of HSFWPB containing VTIOTs. The pore structure changes from closed pores with different sizes→ connected pores with irregular diameters→ irregular collapse pores→ small and uniform circular pores.

(3) The full investment payback period of the project of HSFWPB containing VTIOTs is 1.77 years. At 48.585% of the design output production, the project reaches the break-even point, reflecting strong risk resistance ability.

(4) The combination of the comprehensive utilization of VTIOTs with HSFWPB, the use of appropriate technology and additives to produce high-value-added products can not only improve the utilization rate of VTIOTs, reducing land occupation and environmental pollution, but also improve profits and create considerable economic benefits. The research improves the utilization rate of VTIOTs and provides a new approach to the large-scale application of VTIOTs.

Data availability statement

The original contributions presented in the study are included in the article/Supplementary Material, further inquiries can be directed to the corresponding author.

Author contributions

PB proposes method and writes manuscript; CW proposes and participates in design research and reviews the paper; JJ, YQ, JM, HP, ZL, YoZ, YuZ, and FL participate in design research and reviews paper. All authors contributed to the article and approved the submitted version.

Funding

The authors gratefully acknowledge financial support by the National Key Research and Development Program of China (2021YFC1910605), the Natural Science Foundation of Hebei Province (E2020402079), State Key Laboratory of Solid Waste Resource Utilization and Energy Conservation (SWR-2023-007), Science and Technology Research and Development Plan of China Railway Construction Group Co., Ltd. (No. 22-11b, 22-14b), Handan Science and Technology Research and Development Program (21422111260). The funder was not involved in the study design, collection, analysis, interpretation of data, the writing of this article or the decision to submit it for publication.

Conflict of interest

Authors YZ and FL were employed by the China Railway Construction Group Co., Ltd.

The remaining authors declare that the research was conducted in the absence of any commercial or financial relationships that could be construed as a potential conflict of interest.

Publisher's note

Supplementary material

The Supplementary Material for this article can be found online at: https://www.frontiersin.org/articles/10.3389/feart.2023.1214184/full#supplementary-material

References

Asaeda, T., and Ca, V. T. (2000). Characteristics of permeable pavement during hot summer weather and impact on the thermal environment. *Build. Environ.* 35 (4), 363–375. doi:10.1016/s0360-1323(99)00020-7

Cai, J. W., Lv, N. W., Jia, X. Y., Zhang, R. F., Xu, G. L., Cai, L. X., et al. (2021). Properties of permeable ceramic brick prepared with felsite tailing. *J. Build. Eng.* 44, 103426. doi:10.1016/j.jobe.2021.103426

Chen, D. Q., Cui, Y. F., Li, Z. H., and Iqbal, J. (2021). Watch out for the tailings pond, a sharp edge hanging over our heads: Lessons learned and perceptions from the Brumadinho tailings dam failure disaster. *Remote Sens-basel.* 13 (9), 1775–1796. doi:10.3390/rs13091775

Chen, S. Y., Fu, X. J., Chu, M. S., Liu, Z. G., and Tang, J. (2015). Life cycle assessment of the comprehensive utilisation of vanadium titano-magnetite. *J. Clean. Prod.* 101, 122–128. doi:10.1016/jjclepro.2015.03.076

Chen, T., Jian, S., Xie, X., Zhang, Y., Li, J., Li, B. Q., et al. (2021). Research progress on comprehensive utilization of vanadium-titanium magnetite tailings. *Conserv. Util. Min. Res.* 41 (2), 174–178. doi:10.13779/i.cnki.issn1001-0076.2021.02.023

Fang, M. J., Wang, X., Liu, J. J., Xu, Z. Y., and Chen, Y. M. (2022). Design, application and performance improvement of eco-permeable pavement materials (Eco-PPMs): A review. *Constr. Build. Mater* 360, 129558. doi:10.1016/j.conbuildmat.2022.129558

Gan, C. D., Cui, S. F., Wu, Z. Z., and Yang, J. Y. (2022). Multiple heavy metal distribution and microbial community characteristics of vanadium-titanium magnetite tailing profiles under different management modes. *J. Hazare Mater* 429, 128032. doi:10.1016/j.jhazmat.2021.128032

Guan, X., Wang, J. Y., and Xiao, F. P. (2021). Sponge city strategy and application of pavement materials in sponge city. *J. Clean. Prod.* 303, 127022. doi:10.1016/J.JCLEPRO.2021.127022

Han, J., Wang, C. Q., Demg, S. H., and Lichtfouse, E. (2023). China's sponge cities alleviate urban flooding and water shortage: A review. *Environ. Chem. Lett.* 21, 1–18. doi:10.1007/s10311-022-01559-x

He, B. J., Zhu, J., Zhao, D. X., Gou, Z. H., Qi, J. D., and Wang, J. S. (2019). Co-benefits approach: Opportunities for implementing sponge city and urban heat island mitigation. *Land Use Policy* 86, 147–157. doi:10.1016/j.landusepol.2019.05.003

He, X. M., Duan, X. C., Guo, W., and Cui, W. L. (2023). Experimental study on preparation of sintered permeable brick with high coal gangue content. *Ceramic* 3, 17–20. doi:10.19397/j.cnki.ceramics.2023.03.058

Huang, Y., Zhou, D., Wang, L., Jiao, G. H., Gou, H., Li, Z. J., et al. (2023). Role of tailing colloid from vanadium-titanium magnetite in the adsorption and cotransport with vanadium. *Envir sci Pollut R* 30, 34069–34084. doi:10.1007/S11356-022-24621-1

Jiang, F., Ren, B. Z., Hursthouse, A. S., and Zhou, Y. Y. (2018). Trace metal pollution in topsoil surrounding the xiangtan man-ganese mine area (south-Central China): Source identification, spatial distribution and assessment of potential eco-logical risks. *Int. J. Env. Res. Pub He* 15 (11), 2412–2427. doi:10.3390/ijerph15112412

Jiang, P., Lv, S. W., Wang, Y., Li, N., and Wang, W. (2019). Investigation on direct shear and energy dissipation characteristics of iron tailings powder reinforced by polypropylene fiber. *Appl. Sci-basel.* 9 (23), 5098–5113. doi:10.3390/app9235098

Kim, Y., Lee, Y., Kim, M., and Park, H. (2019). Preparation of high porosity bricks by utilizing red mud and mine tailing. *J. Clean. Prod.* 207, 490–497. doi:10.1016/jjclepro.2018.10.044

Kong, X. F., Shan, Y. X., Zhou, Z. L., Fan, C. G., and Zhang, Y. (2022). Analysis of influencing factors on properties of permeable brick sintered with iron tailings based on orthogonal test. *J. Anhui Univ. Technol. Nat. Sci.* 39 (2), 145–152. doi:10.3969/j.issn.1671-7872.2022.02.004

Li, L., Jiang, T., Zhou, M., and Chen, C. (2020). Overall utilization of vanadium–titanium magnetite tailings to prepare lightweight foam ceramics. *Process Saf. Environ.* 139, 305–314. doi:10.1016/jpsep.2020.04.034

Li, J. H., Li, X. L., Liang, S., Zhang, Y. S., Ye, Q., Zhang, L., et al. (2021). Preparation of water-permeable bricks derived from fly ash by autoclaving. *Constr. Build. Mater* 271, 121556. doi:10.1016/J.CONBUILDMAT.2020.121556

Li, L., Sun, J. W., Jiang, J. J., and Wang, J. (2021). The effect of environmental regulation competition on haze pollution: Evidence from China's province-level data. *Environ. Geochem Hlth* 44, 3057–3080. doi:10.1007/s10653-021-00854-w

Li, L., Jiang, T., Chen, B. J., Wen, J., and Yang, G. D. (2022). Integrated utilization of vanadium-titanium magnetite tailings for synthesis of lightweight foamed ceramics: Effect of chemical composition on the properties and phase evolution. *J. Sustain Metall.* 8, 646–657. doi:10.1007/S40831-022-00517-9

Li, X. S., Li, Q. H., Hu, Y. J., Chen, Q., Peng, J., Xie, Y., et al. (2022). Study on three-dimensional dynamic stability of open-pit high slope under blasting vibration. *Lithosphere-us* 2021, 6426550. doi:10.2113/2022/6426550

Liu, H. J., and Zhao, L. L. (2020). Experimental study on activation of vanadium-titanium magnetite tailings and its use as cement admixture. *Iron Stl Vanadium Titan.* 41 (4), 97–102. doi:10.7513/i.issn.1004-7638.2020.04.018

Liu, Y., Tang, W., and Singh, R. P. (2019). Study on Compressive strength and water permeability of steel slag-fly ash mixed permeable brick. *Appl. Sci-basel.* 9 (8), 1542–1552. doi:10.3390/app9081542

Liu, L., Cheng, X., Miao, X. W., Shi, Y. L., Zhang, M. X., Guo, M., et al. (2020). Preparation and characterization of majority solid waste based eco-unburned permeable bricks. *Constr. Build. Mater* 259, 120400. doi:10.1016/j.conbuildmat.2020.120400

Liu, X. M., Li, B., and Wu, Y. F. (2023). The pretreatment of non-ferrous metallurgical waste slag and its research progress in the preparation of glass-ceramics. *J. Clean. Prod.* 404, 136930. doi:10.1016/j.jclepro.2023.136930

Luo, L. Q., Li, K. Y., Fu, W., Liu, C., and Yang, S. Y. (2019). Preparation, characteristics and mechanisms of the composite sintered bricks produced from shale, sewage sludge, coal gangue powder and iron ore tailings. *Constr. Build. Mater* 232, 117250–250. doi:10.1016/j.conbuildmat.2019.117250

Luo, X., Ren, B. Z., Hursthouse, A. S., Jiang, F., and Deng, R. J. (2019). Potentially toxic elements (PTEs) in crops, soil, and water near Xiangtan manganese mine, China: Potential risk to health in the foodchain. *Environ. Geochem Hlth* 42, 1965–1976. doi:10.1007/s10653-019-00454-9

Luo, P. P., Liu, L. M., Wang, S. T., Ren, B. M., He, B., and Nover, D. (2022). Influence assessment of new Inner Tube Porous Brick with absorbent concrete on urban floods control. *Case Stud. Constr. Mater* 17, e01236. doi:10.1016/J.CSCM.2022.E01236

Lv, R. B., Liang, S., Li, X. L., Hou, H. J., Ke, Y., Li, X. W., et al. (2022). Production of water-permeable ceramic bricks derived from fly ash via a simple pellet method: Mechanism of mechanical strength and permeability. *Constr. Build. Mater* 351, 128989. doi:10.1016/j.conbuildmat.2022.128989

Nguyen, T. T., Ngo, H. H., Guo, W. S., Wang, X. C., Ren, N. Q., Li, G. B., et al. (2019). Implementation of a specific urban water management-Sponge city. *Sci. Total Environ.* 652, 147–162. doi:10.1016/j.scitotenv.2018.10.168

Peng, J. S., Guan, Y. H., Lin, X. J., Xu, X. J., Xiao, L., Wang, H. H., et al. (2020). Comparative understanding of metal hyperaccumulation in plants: A mini-review. *Environ. Geochem Hlth* 43, 1599–1607. doi:10.1007/s10653-020-00533-2

Qi, B. W., Gao, S. W., and Xu, P. L. (2023). The application of rubber aggregate-combined permeable concrete mixture in sponge city construction. *Coating* 13 (1), 87–100. doi:10.3390/COATINGS13010087

Qin, Z., Yao, Y. J., Zhao, J. W., Fu, H. L., Zhang, S., and Qiu, L. Y. (2022). Investigation of migration rule of rainwater for sponge city roads under different rainfall intensities. *Environ. Geochem Hlth* 44, 3395–3407. doi:10.1007/S10653-021-01104-9

Rey, N. J., Demers, I., Bussière, B., Mbonimpa, M., and Gagnon, M. (2020). A geochemical evaluation of a monolayer cover with an elevated water table for the reclamation of the Doyon-Westwood tailings ponds, Canada. *Environ. Earth Sci.* 79, 58–69. doi:10.1007/s12665-019-8797-8

Sansalone, J. J., Kuang, X., and Ranieri, V. (2008). Permeable pavement as a hydraulic and filtration interface for urban drainage. *Irrig. Drain. Eng.* 134 (5), 666–674. doi:10.1061/(asce)0733-9437(2008)134:5(666)

Sarathchandra, S. S., Rengel, Z., and Solaiman, Z. M. (2022). Remediation of heavy metal-contaminated iron ore tailings by applying compost and growing perennial ryegrass (Lolium perenne L). *Chemosphere* 288, 132573. doi:10.1016/j.chemosphere.2021.132573

Seifeddine, K., Amziane, S., and Toussaint, E. (2022). Experimental investigation of physical characteristics to improve the cooling effect of permeable pavements. *Constr. Build. Mater* 345, 128342. doi:10.1016/J.conbuildmat.2022.128342

Shi, L., and Song, X. (2020). Influence of vanadium-titanium magnetite tailings on autoclaved aerated concrete blocks. *Iron Stl Vanadium Titan.* 41 (3), 84–89. doi:10.7513/i.issn.1004-7638.2020.03.014

Song, C. (2022). Application of nature-based measures in China's sponge city initiative: Current trends and perspectives. *Nature-Based Solu.* 2, 100010. doi:10.1016/j.nbsj.2022.100010

Sun, H. Y., Wei, X. F., Sun, X. M., Jia, F. C., Li, D. J., and Li, J. (2021). Bioaccumulation and translocation characteristics of heavy metals in a soil-maize system in reclaimed land and surrounding areas of typical vanadium-titanium magnetite tailings. *Environ. Sci.* 42 (3), 1166–1176. doi:10.13227/j.hjkx.202007200

Sun, Y., Gu, X. W., and Xu, X. C. (2021). Ecological restoration and mechanical reinforcement effect of slope of tailings reservoir. *Environ. Earth Sci.* 80, 80–12. doi:10.1007/s12665-020-09325-4

Tang, Z. E., Deng, R. J., Zhang, J., Ren, B. Z., and Hursthouse, A. (2019). Regional distribution characteristics and ecological risk assessment of heavy metal pollution of different land use in an antimony mining area—xikuangshan, China. *Hum. Ecol. Risk Assess.* 26, 1779–1794. doi:10.1080/10807039.2019.1608423

Tang, Y., Lin, H., Wang, Y. X., and Zhao, Y. (2021). Rock slope stability analysis considering the effect of locked section. *B Eng. Geol. Environ.* 80, 7241–7251. doi:10.1007/s10064-021-02366-4

Wang, X. G., and Qin, L. Y. (2019). Experimental study on preparation of high-strength concrete with vanadium-titanium magnetite tailings. *Iron Stl Vanadium Titan.* 40 (3), 77–82. doi:10.7513/i.issn.1004-7638.2019.03.014

Wang, K., Yang, P., Karen, H. E., Lv, W. S., and Bu, L. (2018). Status and development for the prevention and management of tailings dam failure accidents. *Chin. J. Eng.* 240 (5), 526–539. doi:10.13374/j.issn2095-9389.2018.05.002

Wang, C. L., Ren, Z. Z., Zheng, Y. C., Ye, P. F., Zhang, K. F., and Cui, X. W. (2019). Effects of heat treatment system on mechanical strength and crystallinity of CaO-MgO-Al_2O_3-SiO_2 glass-ceramics containing coal gangue and iron ore tailings. *J. New Mat.* 22 (2), 70–78. doi:10.14447/jnmes.v22i2.a02

Wang, Y. G., Gao, S., Liu, X. M., Tang, B. W., Mukiza, E., and Zhang, N. (2019). Preparation of non-sintered permeable bricks using electrolytic manganese residue: Environmental and NH3-N recovery benefits. *J. Hazard Mater* 378, 120768. doi:10.1016/j.jhazmat.2019.120768

Wang, Z. Y., Guo, J. L., and Li, C. (2019). Study on the preparation and performance of iron tailing-based glass permeable bricks. *Mine Prot. Util.* 34 (4), 66–70. doi:10.13779/j.cnki.issn1001-0076.2019.04.011

Wang, C. L., Li, Y., Cai, H., and Xiao, J. Z. (2021). *New type of concrete based industrial solid waste*. Beijing: Science Press.

Wang, S. X., Zhang, K. F., Zang, S. H., Ye, P. F., Wang, Y. B., Zhai, Y. X., et al. (2021). Preparation and properties study of high-strength sintered permeable brick with multiple solid waste. *Metal. Mine* 9, 206–215. doi:10.19614/j.cnki.jsks.202109029

Wang, C. L., Wang, Z. J., Yang, F. H., and Zheng, Y. C. (2022). *Preparation of new green building materials from tailings and steel slag*. Beijing: Science Press.

Wang, H. F., Liu, Y., and Mei, Z. (2022). Basic physical characteristics of the water-permeable brick with composite structure. *J. Wuhan. Univ. Techonl* 37, 645–655. doi:10.1007/S11595-022-2579-Y

Wang, C. L., Jing, J. L., Qi, Y., Zhou, Y. X., Zhang, K. F., Zheng, Y. C., et al. (2023a). Basic characteristics and environmental impact of iron ore tailings. *Front. Earth Sci.* 11, 1181984. doi:10.3389/feart.2023.1181984

Wang, C. L., Ma, J. T., Yang, F. H., Zhang, G. Q., Chen, J. L., Jing, J. L., et al. (2023b). Preparation and properties of composite cementitious materials containing vanadium-titanium iron ore tailings. *Iron Stl Vanadium Titan.* 44 (1), 98–105. doi:10.7513/j.issn.1004-7638.2023.01.017

Wang, C. L., Qi, Y., Jing, J. L., Ma, J. T., Zhou, Y. X., Ping, H. Y., et al. (2023c). Properties and microstructure of total tailings cemented paste backfill material containing mining and metallurgical solid waste. *Front. Earth Sci.* 11, 1181952. doi:10.3389/feart.2023.1181952

Xi, C. P., Zheng, F., Xu, J. H., Yang, W. G., Peng, Y. Q., Li, Y., et al. (2018). Preparation of glass-ceramic foams using extracted titanium tailing and glass waste as raw materials. *Constr. Build. Mater* 190, 896–909. doi:10.1016/j.conbuildmat.2018.09.170

Xu, Y. S., Shen, S. L., Lai, Y., and Zhou, A. N. (2018). Design of sponge city: Lessons learnt from an ancient drainage system in Ganzhou, China. *J. Hydrol.* 563, 900–908. doi:10.1016/jjhydrol.2018.06.075

Xu, S., Cao, B. Y., Liu, X., Wu, J., Wang, J., and Du, M. L. (2019). Study on preparation of permeable brick by activated sludge doping tailings and its performance. *Non-metallic Min.* 42 (5), 28–30.

Yan, Z. Q., Qing, Z. Q., Guo, M., Yi, G. L., Shi, Y. L., Cheng, F. Q., et al. (2020). Pilot and industrial scale tests of high-performance permeable bricks producing from ceramic waste. *J. Clean. Prod.* 254, 120167. doi:10.1016/j.jclepro.2020.120167

Yang, F., and Sun, X. M. (2020). Preparation of ordinary Portland clinker with vanadium-titanium magnetite tailings. *Iron Stl Vanadium Titan.* 41 (2), 75–81. doi:10.7513/i.issn.1004-7638.2020.02.015

Yang, M., Ju, C. G., Xue, K. R., Peng, Y. Z., Han, H., Wan, Q. Q., et al. (2021). Environmental-friendly non-sintered permeable bricks: Preparation from wrap-shell lightweight aggregates of dredged sediments and its performance. *Constr. Build. Mater* 273, 121751. doi:10.1016/j.conbuildmat.2020.121751

Ye, P. F. (2021). *Preparation and mechanism of high-strength permeable brick from vanadium-titanium iron ore tailings*. Handan: University of Engineering.

Young, G., Chen, Y., and Yang, M. (2021). Concentrations, distribution, and risk assessment of heavy metals in the iron tailings of Yeshan National Mine Park in Nanjing, China. *Chemosphere* 271, 129546. doi:10.1016/j.chemosphere.2021.129546

Yu, X. M., Kang, X., Li, Y. M., Cui, Y. L., Tu, W. G., Shen, T., et al. (2019). Rhizobia population was favoured during *in situ* phytoremediation of vanadium-titanium magnetite mine tailings dam using Pongamia pinnata. *Environ. Pollut.* 255, 113167. doi:10.1016/j.envpol.2019.113167

Yu, T. J., Liu, D. G., Zhang, H. T., and Wang, H. D. (2021). Influence of pore water phase change on service performance for permeable pavement in sponge city. *Water Sci. Technol.* 84 (12), 3769–3779. doi:10.2166/WST.2021.459

Zhang, X., Yang, H., and Cui, Z. (2018). Evaluation and analysis of soil migration and distribution characteristics of heavy metals in iron tailings. *J. Clean. Prod.* 172, 475–480. doi:10.1016/j.jclepro.2017.09.277

Zhang, Y., Zhang, T. A., Dreisinger, D., Lv, C. X., Lv, G. Z., and Zhang, W. G. (2019). Recovery of vanadium from calcification roasted-acid leaching tailing by enhanced acid leaching. *J. Haz Mat.* 369, 632–641. doi:10.1016/j.jhazmat.2019.02.081

Zhang, J. J., Liu, B., and Zhang, S. G. (2021). A review of glass ceramic foams prepared from solid wastes: Processing, heavy-metal solidification and volatilization, applications. *Sci. Total Environ.* 781, 146727. doi:10.1016/j.scitotenv.2021.146727

Zhang, H. Z., Qi, Y., Jing, J. L., Wang, C. L., Zhou, Y. X., Zhang, K. F., et al. (2023). Properties and environmental impact of building foundation pit backfilling materials containing iron and steel solid waste. *Front. Earth Sci.* 11, 1181974. doi:10.3389/feart.2023.1181974

Zhao, X., Fourie, A., and Qi, C. C. (2020). Mechanics and safety issues in tailing-based backfill: A review. *Int. J. Min. Met. Mater* 27 (9), 1165–1178. doi:10.1007/s12613-020-2004-5

Zhu, X. Y., Sun, N., Huang, Y., Zhu, Y. G., and Wang, W. Q. (2021). Preparation of full tailings-based foam ceramics and auxiliary foaming effect of vanadium-titanium magnetite tailings. *J. Non-Cryst Solids.* 571, 121063. doi:10.1016/j.jnoncrysol.2021.121063